Mechanical and damping properties of graphene-reinforced CuAlMn matrix laminated composites

Dongxuan Li[1,2], Xiaosong Jiang[1,2*], Hongliang Sun[1,2], Tianyan Liu [3*], Zixuan Wu[4], Liu Yang[5]

[1]Key Laboratory of Advanced Technologies of Materials, Ministry of Education, Chengdu 610031, China [2]School of Materials Science and Engineering, Southwest Jiaotong University, Chengdu Sichuan 610031, China

[3]Reactor Engineering Research Sub-institute, Nuclear Power Institute of China, Chengdu 610005, People's Republic of China

[4]School of Engineering and Materials Science, Queen Mary University of London, London E1 4NS, United Kingdom

[5]Institute for Applied Materials (IAM-WK), Karlsruhe Institute of Technology (KIT), Karlsruhe 76131, Germany

***Corresponding author:** xsjiang@swjtu.edu.cn (**X.S. Jiang**) OR rexroi@hotmail.com (T.Y. Liu).

Abstract

Graphene (GR)/Cu-11.9Al-2.5Mn composites with bionic laminar structure were prepared by vacuum hot pressing method using flake metallurgy, and the effects of graphene content on the microstructure, mechanical properties and damping properties of the composites were investigated. The results showed that the addition of 0.25 wt.% graphene increased the tensile strength and hardness by about 17% and 27%, respectively, which was attributed to the effective load-transferring mechanism of the graphene uniformly dispersed in the matrix, and the increase in the dislocation density caused by thermal expansion mismatch also affected the mechanical properties. Meanwhile the damping properties of 0.25 wt.% graphene samples were significantly improved, which was attributed to the introduction of the enormous dislocations and micro interfaces by the addition of graphene, and a significant amount of energy was dissipated by the dislocation motion, GR/matrix interfacial sliding, and frictional

sliding between the graphene layers. Therefore, it can be concluded that both mechanical and damping properties enhancement mechanisms are related to dislocation behavior and interfacial bonding, and the addition of an appropriate amount of graphene can achieve a balance between mechanical and damping properties.

Keywords

Laminar structure, Graphene, Mechanical properties, Damping properties

1. Introduction

Damping is the behavior of a material that dissipates mechanical vibration energy in the form of thermal energy. Damping materials can improve the service life of dynamic structures, reduce noise pollution, and are widely used in construction, aerospace, and medical fields [1, 2]. Cu-based alloys are commonly used as a kind of damping alloys with low production costs, good thermal stability, and a wide range of adjustable phase transition temperatures, among which CuAlMn alloys are more suitable for industrial applications due to their excellent ductility and cold workability [3]. It can be used in the manufacture of medical guidewires by obtaining a gradient structure that gives different properties to the end and the tip, and also has a wide range of applications in sensors and controllers for vehicles [4, 5]. However, the lower strength of CuAlMn alloys limits their applications, how to improve the strength while maintaining the toughness of the alloys is a difficult problem. In addition, the damping peaks of CuAlMn alloys mainly appear in the region of thermoelastic martensitic phase transition, but the damping materials are usually applied in constant temperature conditions (e.g., room temperature) [6], the lack of energy dissipation of the phase transition makes the alloy's damping greatly reduced, and it is necessary to play the other mechanisms to improve the damping properties, but improving both damping properties and mechanical properties at the same time is also a major difficulty because the damping properties and mechanical properties have opposite trends [7].

Composites are expected to obtain excellent comprehensive properties, and it has now been shown that doping of reinforcing phases into the alloys can greatly improve dislocation damping and interfacial damping. For instance, in reduced graphene oxide (RGO)/Al-Mg-Si composites [8], RGO increases the dislocation density within the

matrix and the RGO/Al interface facilitates the formation of precipitated phases, lowering the energy barrier for the formation of stacking faults, which lead to a great improvement in damping properties; and in carbon fiber/resin composites doped with graphene nanoplatelets (GNPs) [9], the sliding friction at the GNPs/resin interface dissipates a considerable amount of energy and the damping properties is significantly improved due to the large specific surface area of the GNPs and the weak interfacial bonding with the resin. In addition, the effect of reinforcement on mechanical properties has also been widely investigated, for example, Chen et al. [10] explored the physical properties of GR/Cu matrix composites, where the yield strength could be increased from 142 MPa to 310 MPa under the reinforcing mechanisms such as grain refinement and load transfer. Recently, Jiao et al. [11] prepared multilayer graphene (MLG)/CuAlMn composites via packaged hot roll bonding process, and the results showed that MLG could realize the simultaneous enhancement of damping properties and mechanical properties. Therefore, the doping of reinforcing phase is a feasible method for the damping material to obtain excellent comprehensive properties.

It can also be found in the study of Jiao et al. [11] that MLG not only achieves a balance between damping and strength, but also improves the toughness at the same time. However, for general metal matrix composites, it is difficult to maintain good toughness while obtaining high strength, as shown in the results of Chen et al. [10], the increase in strength is accompanied by a significant decrease in plasticity, and the fracture mode is changed from ductile fracture to brittle fracture. The nacreous layer of shells in nature provides ideas to solve this problem, researchers found that the shells can have both high strength and toughness is that it takes the hard inorganic material flakes as "bricks", and the flexible organic material as "mortar" to fill in between the flakes so as to build up an orderly "brick-mortar" structure, where the hard phase provides strength, and the sliding of the lamellae, the flakes of the cracks of the deflection and the bridging role of the toughness increased [12-14]. The bionic laminar structure is proposed with reference to nacreous layers to achieve better mechanical properties by stacking soft and hard materials in layers.

In summary, the selection of graphene as the reinforcing phase to construct

laminated metal matrix composites might balance the relationship between damping, strength and toughness. There are numerous methods to prepare laminated composites, of which sheet powder metallurgy is a simple and fast process [15], the flake morphology provides more attachment points for graphene [16], and graphene can have a better bonding with the matrix under the impact of abrasive balls, which solves the problem that graphene is difficult to be dispersed homogeneously in the metal matrix [17]. The laminated composite powder is then subjected to a hot-press sintering process, which allows the graphene and the flake powder to be aligned perpendicular to the direction of pressure under gravitational self-assembly, thus realizing a laminar structure. In this paper, GR/CuAlMn laminated composites are prepared by flake powder metallurgy and vacuum hot pressing method, which is expected to synthesize the reinforcing effect of graphene on mechanical and damping properties, while maintaining the good toughness of CuAlMn alloy under the effect of laminar structure.

2. Experimental

2.1. Material preparation

In this paper, $(Cu\text{-}11.9Al\text{-}2.5Mn)_{1-x}GR_x$ (x = 0, 0.25, 0.5, 1, wt.%) composites with different graphene contents were prepared, and the raw materials used were Cu powder (250 mesh), Al powder (300 mesh), Mn powder (300 mesh) and graphene. In order to ensure that graphene can be dispersed uniformly in the matrix, the surface of graphene needs to be modified first. Initially, sodium dodecyl sulfate (SDS) and graphene were poured into deionized water and stirred homogeneously, ultrasonication was used to allow SDS to fully combine with graphene, then repeated filtration was performed to remove excess SDS, and finally dried for 24 h to obtain the modified graphene.

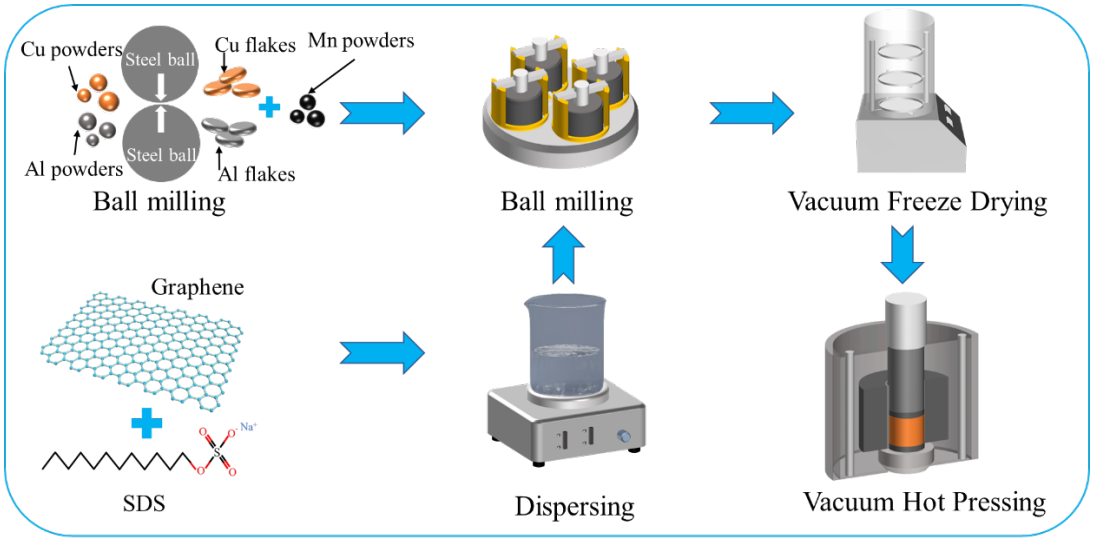

Fig. 1. Schematic diagram of the preparation process of GR/CuAlMn laminated composites

The Cu powder was put into a planetary ball mill with tert-butanol as the ball milling medium, and steel balls were used to grind it at 300 rpm, 20:1 ball material ratio for 6 h to obtain flake Cu powder, flake Al powder was obtained by grinding the spherical Al powder for 3 h in the same process. The flake Cu powder, Al powder and Mn powder were mixed with different content of graphene, and mixed with onyx balls in a planetary ball mill at 300 rpm with 1:1 ball ratio for 1 h to ensure the uniform dispersion of each element, and the mixed slurry was put into a vacuum freeze dryer for 24 h. The composite powder was then put into a graphite mold, and sintered with a vacuum hot press with sintering parameters of 850 °C, 27 MPa and holding time of 1 h. The blocks with a diameter of 55 mm and a height of 10 mm were obtained under furnace cooling conditions, the methodology is shown in Figure 1.

2.2. Material characterization

Scanning electron microscopy (SEM, ZEISS Sigma 300) was used to observe the microscopic morphology of the blended powders and sample cross sections, and combined with energy dispersive spectroscopy (EDS) to obtain elemental distributions. The phase composition of the composites was determined using an X-ray diffractometer (XRD, Rigaku XRD-6100), and the microstructure and phase composition of the samples were further analyzed using a transmission electron microscope (TEM, FEI Talos F200X). The density of the samples was determined using the Archimedes

drainage method and hardness was determined using the microhardness tester (HXD-100TM/LCD). The tensile strength of the samples was tested using a universal testing machine (WDW-3100) at 0.5 mm/min and the tensile fracture morphology was observed under a scanning electron microscope. The room temperature damping properties of the specimens were tested using a dynamic mechanical analyzer (DMA, TA DMA850) with a frequency of 1 Hz and an amplitude range of 1-600 μm.

3. Results

3.1. Microscopic morphology of composite powders

The microscopic morphology of the composite powder is shown in Fig. 2. Metal flakes of different sizes can be observed from Fig. 2a-c, the formation of flake morphology occurs in the first stage of ball milling, in which the particles are plastically deformed, fractured, cold-welded, and gradually become flake under the extrusion of the steel ball, the weak and curled parts of the edges flake off into small particles under the impact (Fig. 2b) and are laminated to the surface of the powder under the action of cold-welding [18] (Fig. 2b). However, cold welding should be avoided as much as possible during ball milling of flake powders to reduce particle agglomeration and clustering to ensure uniform flake morphology [19]. The use of tert-butanol as a ball milling medium reduces the surface energy and the collision energy of the steel balls to reduce the degree of cold welding, thus ensuring the integrity of the flake morphology.

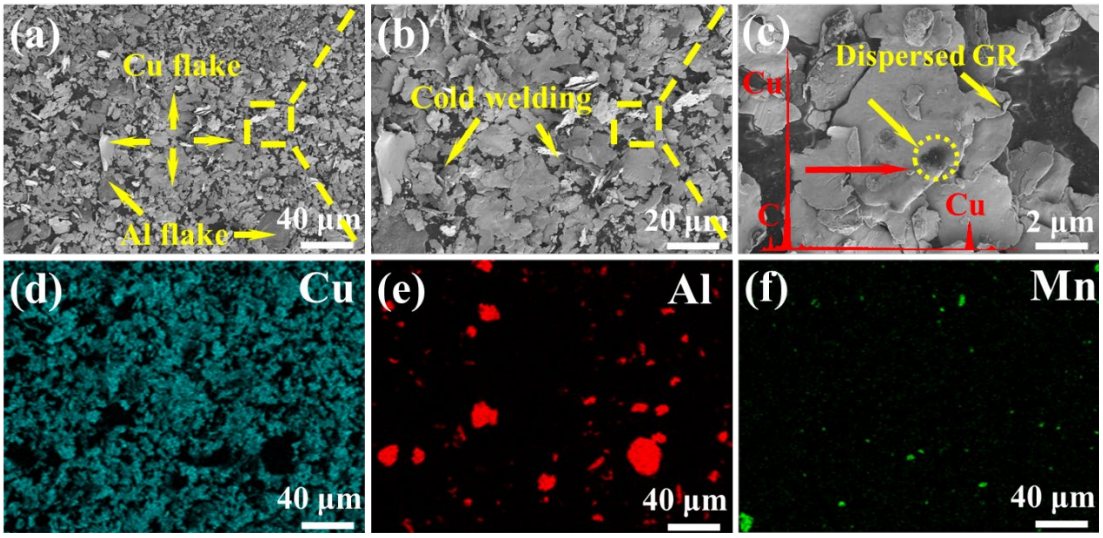

Fig. 2. SEM images of composite powders: (a-c) micro-morphology of CuAlMn + 0.25% GR powder, (d-e) elemental distribution of CuAlMn + 0.25% GR powder

From the EDS plots (Fig. 2d-f), it can be seen that each powder is mixed uniformly, and both Cu and Al powders are in the form of thin flakes, Mn powder is hard and very low in content, so it is mixed directly with the original powder, which is still in the form of small particles. From Fig. 2c, it can be observed that graphene is attached to the surface of Cu flakes under the impact of ball milling, indicating that ball milling can promote the combination of graphene and metal matrix. Cu flakes and Al flakes with large specific surface area provide more attachment points for graphene, which can realize the uniform dispersion of graphene. Because elemental redispersion does not occur during the sintering process, uniform mixing of the powder is the key to ensure the uniformity of the block composition.

3.2. (CuAlMn)1-xGRx composite micro-morphology and phase composition

In order to analyze the effect of graphene content on the phase composition of Cu-11.9Al-2.5Mn alloys, X-ray diffractometer was used to determine the phase composition of each sample (Fig. 3). The diffraction pattern shows that the alloy is mainly composed of α-phase, γ_2-phase and martensitic phase (β_1' and γ_1') at room temperature, α is a solid solution formed by the dissolution of Al atoms into Cu with FCC structure, while γ_2 is a solid solution based on electronic compounds with BCC structure, and the martensitic phases are all monoclinic[7]. The presence of martensitic phase can still be detected under the condition of cooling with the furnace, which can be explained by the fact that Mn element can broaden the β-phase region, improve the stability of the β-phase, reduce the eutectoid reaction temperature of Cu-Al alloy, and shift the eutectoid point to the right [20]. Therefore, after the addition of a certain amount of Mn element, the $\beta \rightarrow \alpha + \gamma_2$ eutectic reaction cannot be carried out completely, allowing a small amount of β-phase to be retained without heat treatment and finally transformed into martensitic phase [21].

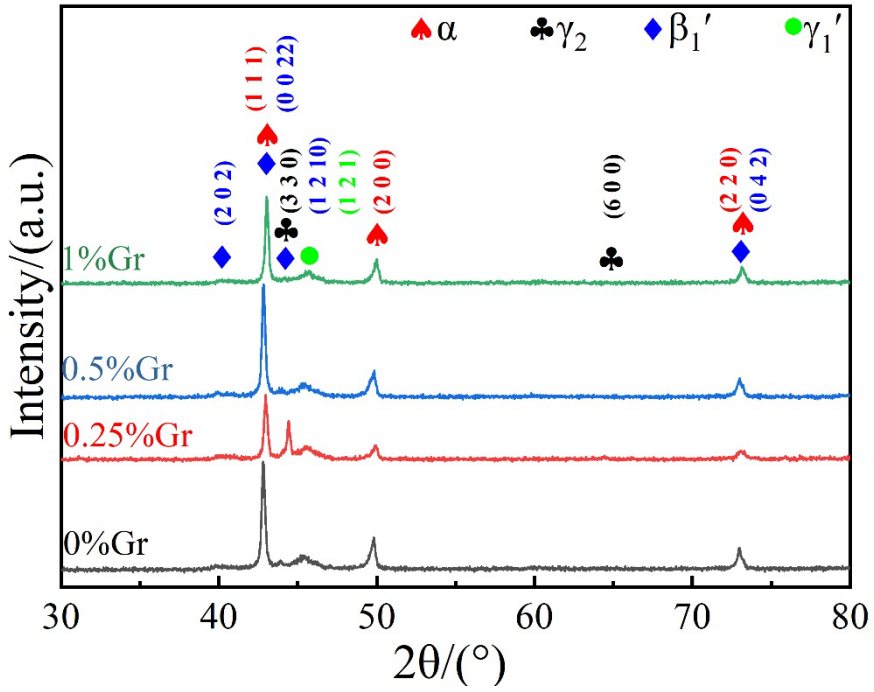

Fig. 3. XRD patterns of samples with different graphene contents

The diffraction peaks of graphene were not observed in the composites, which may be due to the content of graphene being too low and below the detection range of the XRD instrument, or it may be masked by the high intensity diffraction peaks of the α-phase, which was also mentioned in the studies of graphene-reinforced Cu-based composites by Salvo [22] and Gao [23]. Although the phase compositions of the samples with different graphene contents are the same, the peak around 44.5° is significantly higher in the sample containing 0.25 wt.% graphene, probably because graphene introduces defects and causes internal stresses in the matrix, which promotes martensitic nucleation and transformation [24], however, graphene also hinders the migration of grain boundaries and dislocations, so the decrease of this peak may be due to the fact that the higher amount of graphene hinders the martensite transformation [25].

The cross sections of the samples were observed and analyzed using SEM (Fig. 4) and the energy spectra of the samples containing 0.25 wt.% graphene were selected, from which it can be seen that there is a uniform distribution of the individual elements and the black areas are graphene. By observing the SEM photos of the four samples, it is found that there is still a uniformly distributed black phase in the alloy without graphene (Fig. 4a). Distinguishing the phase of the black area in the composite material

is necessary. As shown in Fig. 4(a_1, b_1, c_1, d_1), the intensity of the Cu element in the γ_2-phase decreases and the Al content increases, while the other elements remain unchanged. In addition, the decrease in the content of other elements and the significant increase in the intensity of C element represent the region as graphene. Graphene is distributed in layers in the composites (Fig. 4b-d), and severe agglomeration is found in the sample containing 1 wt.% graphene (Fig. 4d). No obvious voids are found on the surface, which suggests a better densification, and this is in Fig. 7a can be confirmed.

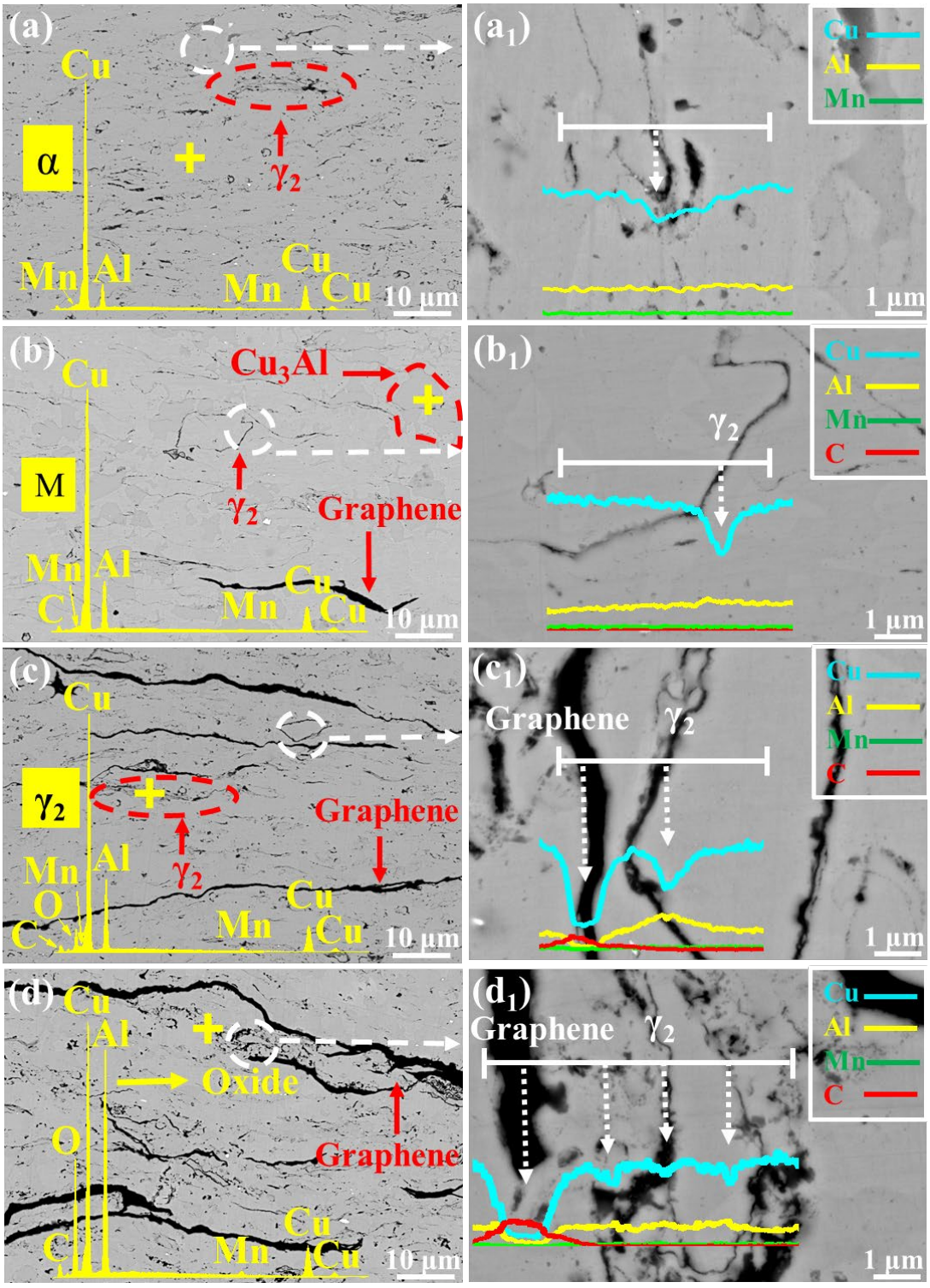

Fig. 4. Micro-morphology and elemental distribution of samples with different graphene contents: (a, a_1) 0 wt.% GR, (b, b_1) 0.25 wt.% GR, (c, c_1) 0.5 wt.% GR, (d, d_1) 1 wt.% GR

In order to analyze the microstructure, X-ray spectroscopy point scanning was done on some areas. Combined with the XRD results, the morphology and distribution of the phases can be roughly confirmed. The light-colored area with the lowest Al

content is the Cu-rich phase(α-phase); the slightly darker area has a slightly higher Al content, which is presumed to be the martensitic phase; the coarser black streaks are the graphene, and the fine black streaks have a relatively high Al content, which is presumed to be the precipitated γ_2-phase. In addition to this black mesh region was also observed (Fig. 4a, c, d), the EDS results showed a significant increase in the Al content in the precipitates and O atoms were detected, it can be speculated that there are more Al oxides in this region, which may be the introduction of O element during the ball milling process.

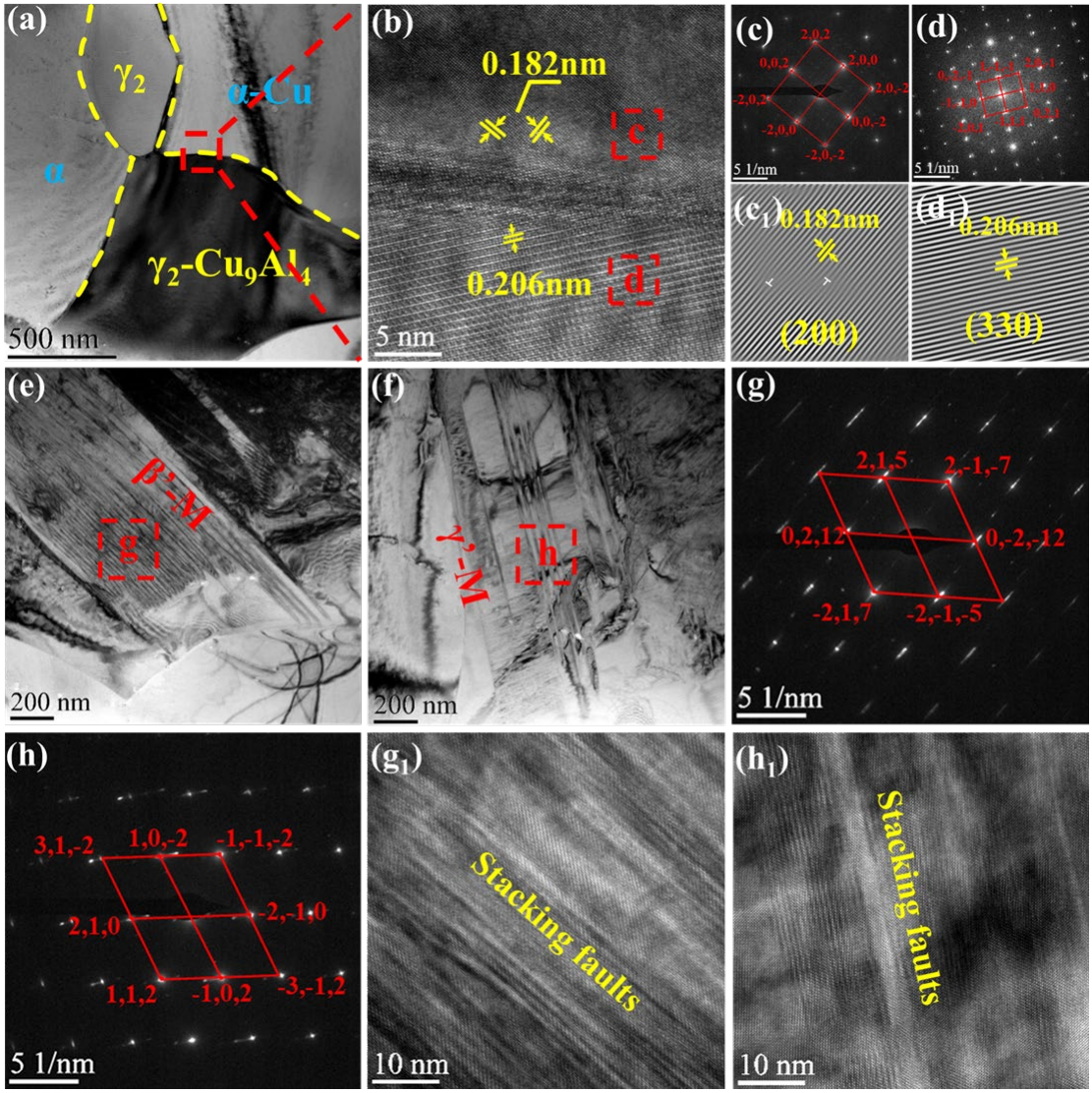

Fig. 5. TEM images of CuAlMn + 0.25% GR samples: (a) morphology of α-phase and γ_2-phase, (b) high-resolution images at the phase interface, (c, d) selected electron diffraction patterns of α-phase and γ_2-phase, (c_1, d_1) IFFT maps of α-phase and γ_2-phase, (e-h) martensite morphology and selected zone electron diffraction patterns,

(g_1, h_1) high-resolution images of martensite

The microscopic morphology of the 0.25 wt.% graphene sample was further observed using TEM. Fig. 5a-d shows the morphology and SAED images of α phase and γ_2 phase. The results show that the α-phase has an FCC structure, while the γ_2 phase has a BCC structure, which is consistent with what has been mentioned in the literature [26], the crystal plane spacing of the α-phase and the γ_2 phase are 0.184 nm and 0.248 nm, respectively, and the large difference in the crystal plane spacing of the two phases results in the chaotic arrangement of the atoms at the phase interfaces, and a small number of dislocations can also be observed in the side of the α-phase (Fig. 5c_1). As shown in Fig. 5e and f, there are two different types of martensite phases in the matrix, the martensite is in the form of thin stripes in Fig. 5e, and the martensite is in the form of thick laths in Fig. 5f, which can be identified as β_1' martensite γ_1' martensite, respectively, based on the diffraction spots. Theoretically, both β_1' and γ_1' martensite are orthorhombic, but the difference in the radii of Cu, Al, and Mn atoms transforms the orthorhombic structure into a monoclinic structure [27]. From the high-resolution images (Fig. 5g_1 and h_1) one can see a high density of streaks, which are stacking faults formed by shearing of the parent phase lattice during the phase transformation process, constituting the sub-structure of the martensite [28], and therefore the diffraction spots are significantly elongated. These two types of martensite by the same parent phase β_1 transformation, and γ_1' corresponding to the formation of Al content of 13 wt.%-14 wt.% of the interval, it is possible that the precipitation of the γ_2 phase is reduced by the action of the Mn element, and many Al elements remain in the parent phase to form an Al-rich region, which can then form the γ_1' phase [27].

Figure 6 shows the morphology and distribution of graphene in the 0.25 wt.% graphene sample. As shown in Fig. 6a, part of the graphene will be distributed along the grain boundaries, which have a hindering effect on the migration of the grain boundaries, and Fig. 6b shows a high-resolution image of graphene, it is observed that the graphene is roughly 7 nm thick, with no impurities or voids at the interface, indicating a good interfacial bonding between graphene and the matrix, whereas Fig. 6e shows the state of the graphene stack, which is roughly 30 nm-50 nm thick, and the

edges of the graphene layers can be observed from the high-resolution image (Fig. 6f), with the measured layer spacing of about 0.336 nm. Fig. 6d shows the IFFT image of the matrix side, it can be seen that there are more dislocations in the matrix, which is due to the large thermal expansion mismatch between the graphene and the matrix (the coefficient of thermal expansion of the CuAlMn alloy and the graphene are 16×10^{-6} k^{-1} and 0.9×10^{-6} k^{-1} , respectively), and the induced thermal stresses cause the plastic deformation of the matrix, thus generating more dislocations near the interface [24].

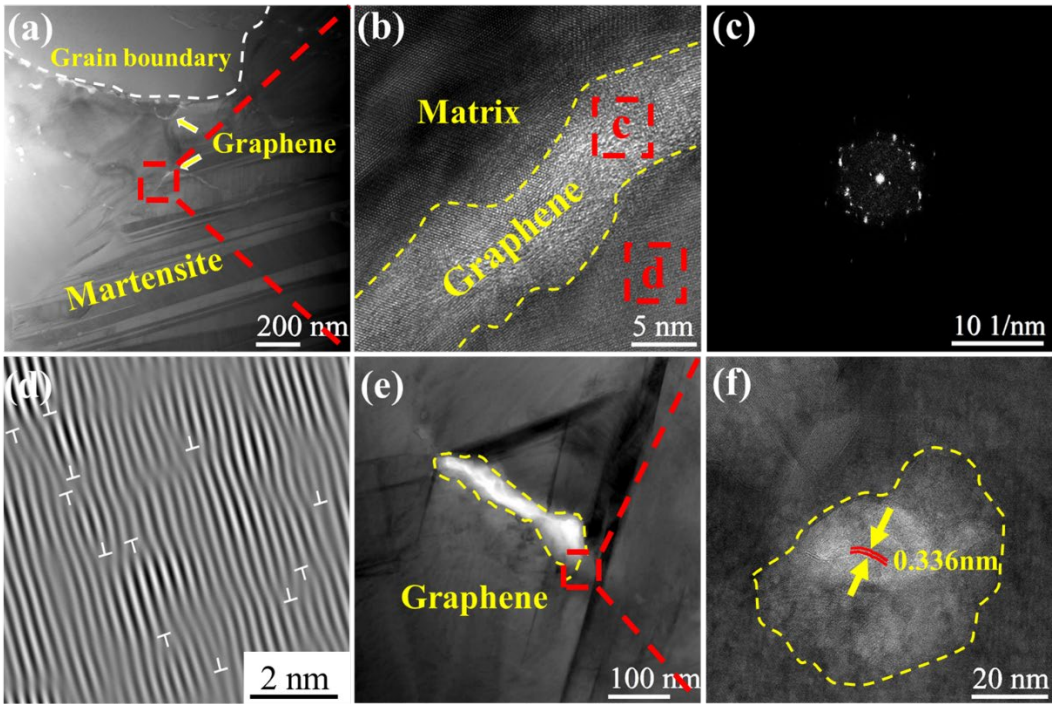

Fig. 6. TEM images of CuAlMn + 0.25% GR samples: (a) low magnification images, (b, c) high resolution images and FFT maps of graphene, (d) IFFT maps of one side of graphene/matrix interface, (e-f) low magnification images and high magnification images of graphene

3.3. (CuAlMn)1-xGRx Mechanical properties of composites

As shown in Fig. 7a, the densification of the alloy is 97%, which gradually decreases with the increase of graphene content, but the minimum is still 95%, and the material can be considered to be dense. The tensile strength and hardness of the material were tested several times and the average values were obtained to plot graphs and bar graphs (Figure 7). From Fig. 7b, it can be seen that the material containing 0.25 wt.% graphene has the highest hardness and the error is larger, while the other three groups

of samples have not much difference in hardness values, it is presumed that the graphene content has less influence on the hardness, and the change of hardness may be mainly related to the number of β_1' phase, the XRD part of the samples analyzed in 0.25 wt.% graphene samples have a higher number of β_1' phase is more in number and the hardness of β_1' phase is higher relative to α phase, so the hardness value increases significantly in the β_1' phase region. As the content of graphene increases, the elongation at break of the material decreases gradually and the tensile strength shows a tendency of increasing and then decreasing (Fig. 7c and d). Tensile properties data are listed in Table 1. The tensile strength of the alloy is about 366 MPa, after addition of 0.25 wt.% graphene, the material strength reaches 423 MPa, which is an increase of about 17%, and the yield strength was increased by about 12% (from 228 to 256 MPa), which, compared to the results of the previous study of the effect of alloying elements on the properties of CuAlMn-based alloys [29], the composites showed further strength and elongation enhancement. When the content of graphene was increased to 0.5 wt.%, the tensile strength decreased significantly, but the yield strength was still higher than that of the alloy.When the content was increased to 1 wt.% the tensile strength of the material was only 314 MPa, which was much lower than that of the alloy.

Graphene content	Tensile strength(MPa)	Yield strength(MPa)	Elongation(%)
0 wt.%GR	366.24	228.70	17.03
0.25 wt.%GR	423.89	256.76	16.61
0.5 wt.%GR	358.98	229.66	17.03
1 wt.%GR	314.88	219.05	15.58

Table 1. Average tensile strength, yield strength and elongation of composite materials

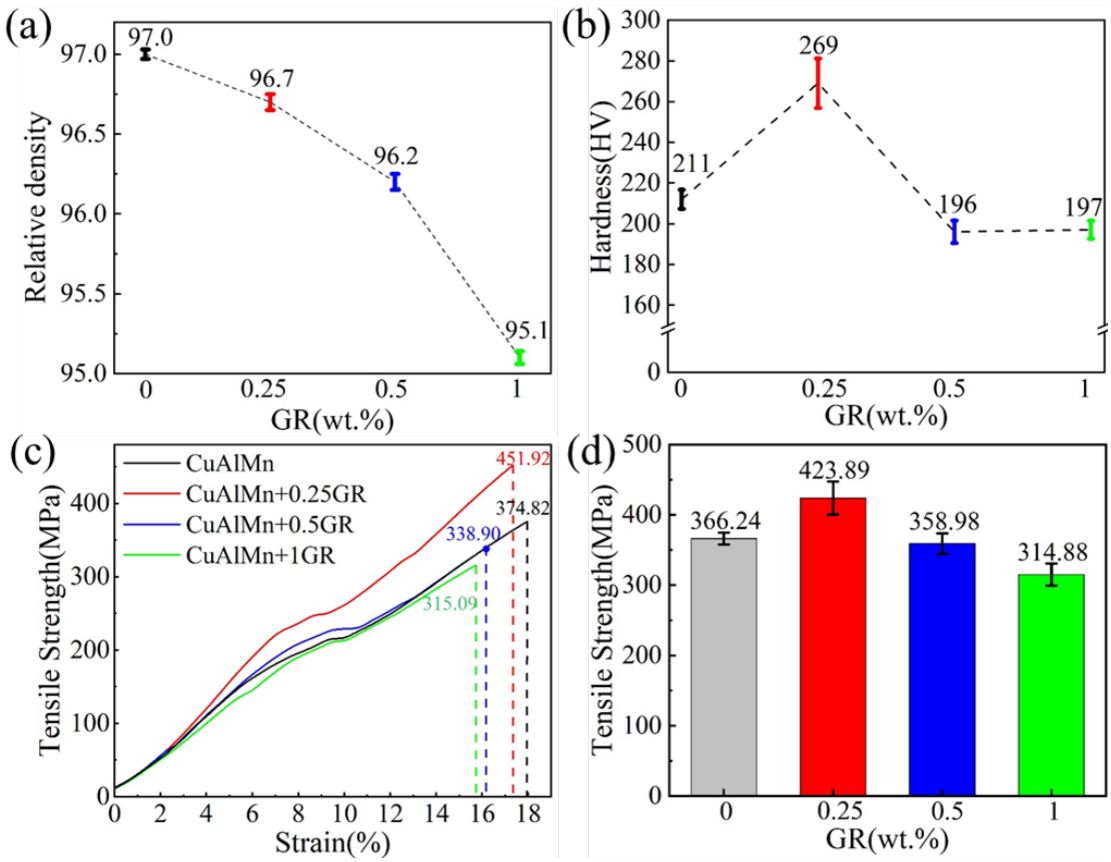

Fig. 7. (a, b) Density and microhardness of composites, (c, d) stress-strain curves of composites and histograms of average tensile strength

A small amount of graphene dispersed within the matrix is homogeneous, which can effectively transfer loads and impede crack extension to improve the strength of the material [30], while too much graphene content results in agglomeration, causing an increase in the number of defects within the material and leading to a gradual decrease in strength and elongation. Theoretically the tensile strength of a composite can be calculated from the following equation [31]:

$$\sigma_c = \sigma_{CuAlMn} v_{CuAlMn} + \sigma_{GR} v_{GR} \quad (1)$$

where σ_c, σ_{CuAlMn}(~ 366 MPa), σ_{GR}(~ 130 GPa [32]) are the tensile strengths of the composites, CuAlMn matrix and graphene, and v_{CuAlMn}(99.2%), v_{GR}(0.8%) are the volume fractions of the CuAlMn matrix and graphene. However, the actual strength of the 0.25 wt.% graphene material is much smaller than the theoretical strength(~ 1400 MPa), which may be attributed to the fact that the alignment of graphene is not always perpendicular to the loading direction, and some agglomeration phenomena and internal defects also cause the strength to be reduced [23, 31].

3.4. Fracture behavior

Fig. 8 displays the fracture morphology of the samples to analyze the effect of graphene content on laminar structure and failure mode. Fig. 8(a, b) are the fracture morphology SEM images of CuAlMn alloy, where a large number of dimples as well as cracks parallel to the layer direction can be observed at high magnification. Fig. 8c shows the macroscopic morphology of the fracture of the 0.25 wt.% graphene sample, where the laminar structure is less obvious because of the low content of reinforcing phase. Fig. 8d shows the microscopic morphology of the 0.25 wt.% graphene sample, the fracture is bright and smooth, small and shallow dimples are observed in a few areas, the graphene embedded in the matrix is observed at the fracture, and there is a crack perpendicular to the layer direction above the graphene, whereas the fracture strength of the single-layer graphene is about 130 GPa, which is much higher than that of the CuAlMn matrix [32], so that the graphene can effectively impede the crack extension and change the expansion path (Fig. 8d), increasing the energy required for fracture. With the increase of graphene content, the laminar structure is more obvious (Fig. 8e, g), and a magnified observation of the graphene-containing region (Fig. 8f, h) shows a more serious agglomeration phenomenon, where stacked graphene is detached from the matrix, with cracks at the interface, and a delamination of graphene, too. This is due to the fact that the weak van der Waals bonds between graphene are more likely to be broken under shear stress, the separation of graphene leads to a reduction in the effective cross-section of the specimen, and can result in a concentration of stress at the graphene/matrix interface, leading to cracks preferentially sprouting at the interface [33], followed by a rapid expansion along the interface, which leads to weakening the bonding of the graphene to the matrix, and ultimately to the pullout of the graphene from the matrix, causing the material to fail.

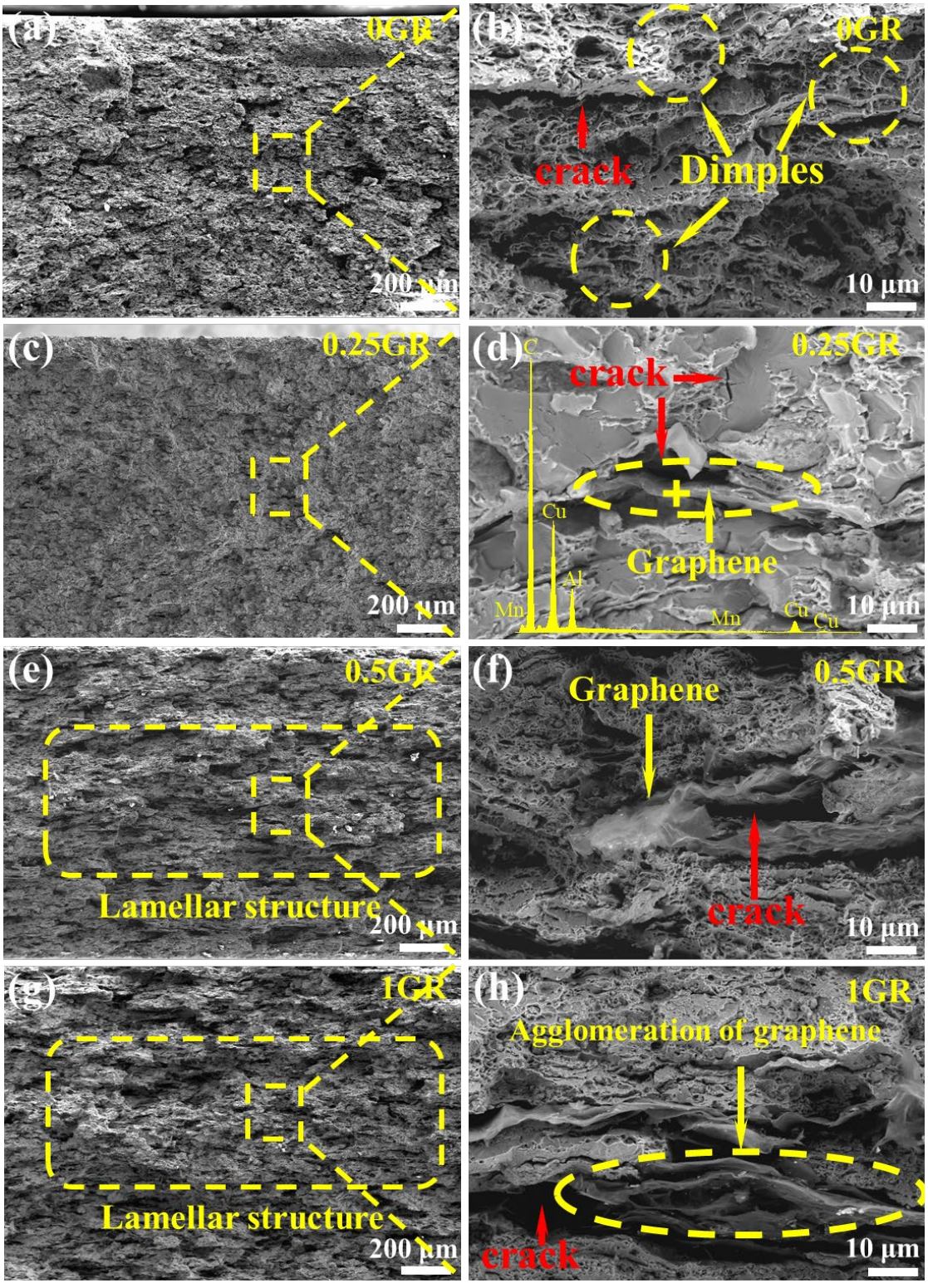

Fig. 8. (a, b) Macroscopic morphology of CuAlMn alloy fracture, (c-h) fracture micromorphology of composites with different graphene contents

3.5. (CuAlMn)1-xGRx Damping properties of composites

Figure 9 shows the room temperature damped strain curves and storage modulus

curves of the samples at 1 Hz frequency. The trend of the damped strain curves for each sample increases with increasing amplitude. The damping value grows rapidly at low amplitude (around 100 μm) and slows down in the 100 μm-400 μm amplitude interval, and the damping value of the alloy reaches its maximum around 400 μm. After the amplitude exceeds 400 μm, the damping values of the alloys begin to decrease slowly, the slope of the curves decreases for the 0.25 wt.% graphene samples and 0.5 wt.% graphene samples, and the increasing trend of the damping values for the 1 wt.% graphene samples is relatively stable. When the amplitude reaches 600 μm, the damping value of the 1 wt.% graphene sample reaches 0.03, which is a 45% improvement compared to the alloy. The storage modulus reflects the stiffness of the material [34], which increases slightly for the 0.25 wt.% graphene samples, while the 1 wt.% graphene samples have much lower storage modulus than the alloys, indicating that a small amount of graphene improves the stiffness of the alloys, but too much graphene leads to a decrease in stiffness. The storage modulus is inversely correlated with the tangent, and the storage modulus decreases with increasing amplitude, which is consistent with the damped strain curve. Compared with the previous results [29], the damping values of the composites are also further improved at a frequency of 1 Hz and 600 μm amplitude.

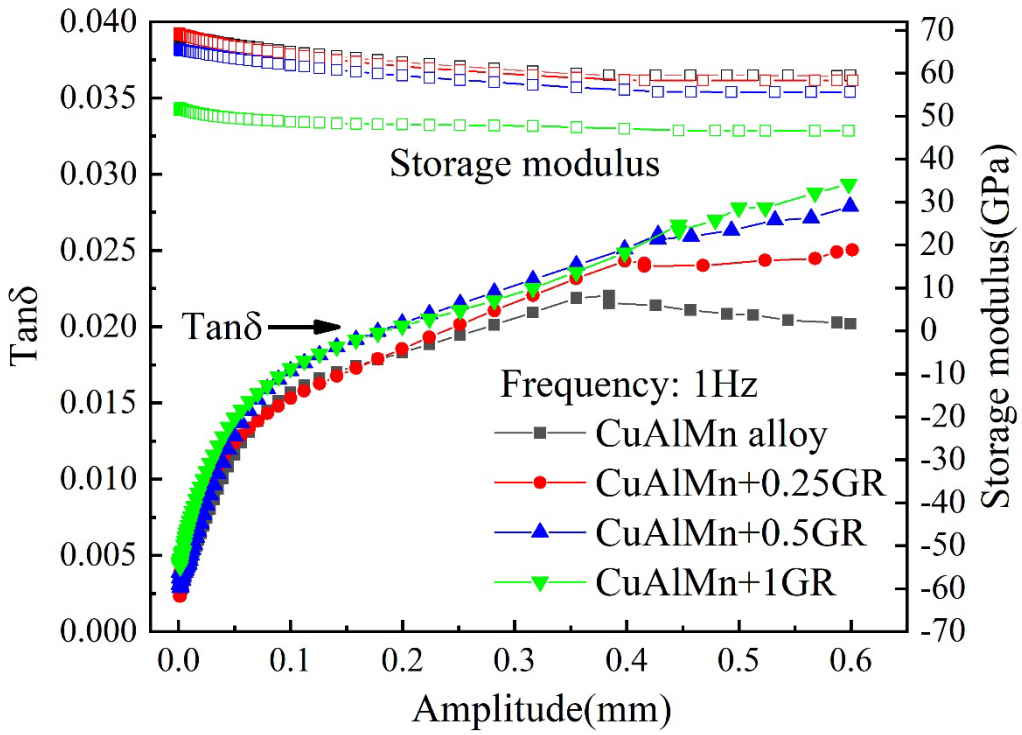

Fig. 9. Damping strain curve versus storage modulus curve for composite materials

From the results, it can be seen that the addition of graphene can effectively improve the damping properties of the samples because graphene introduces a large number of microscopic interfaces and defects. At low amplitude, the damping mechanism is dominated by dislocation damping, and the higher number of dislocations means that there are more movable dislocations at low amplitude [35], so the damping value will be increased after adding graphene. With the increase of amplitude, a large number of dislocations get out of the binding of weak pinning points, and the damping value grows rapidly. After the amplitude increases further, the dislocations interact with each other to form the dislocation entanglement, which makes the number of strong pinning points increase and restricts the dislocation movement, and thus the growth rate of damping decreases. The reason why the damping value of the alloy starts to decrease at high amplitudes may be due to the microplastic deformation of the alloy and the dislocation motion is blocked [36], whereas in composites, the graphene/matrix interface starts to slide at high amplitude regions, and hence the damping value continues to increase.

4. Discussion

4.1. Mechanical properties enhancement mechanisms

The main strengthening mechanisms for composites are broadly load transfer, dislocation strengthening, fine grain strengthening and Orowan strengthening. Load transfer is an important strengthening mechanism of graphene, and the load transfer effect depends on the bond strength of the matrix-graphene interface [37]. As shown in Fig. 8b, when the graphene content is 0.25 wt.%, the graphene in the matrix is uniformly distributed in the form of monolayer or fewer layers, and it can be seen from Figs. 6b and e that there is a good interfacial bonding between graphene and matrix in the 0.25 wt.% graphene sample. Assuming that all graphene is parallel to the loading direction, the contribution of load transfer to strength can be evaluated according to the following equation [38]:

$$\Delta\sigma_{lt} = V_{GR}(\frac{S}{A})(\frac{\tau_m}{2}) \quad (2)$$

τ_m is the shear strength of the CuAlMn alloy, V_{GR} is the volume fraction of graphene, S and A are the interfacial area and cross-sectional area of graphene, where $S = 2(w + t)I_{GR}$ and $A = wt$ (w, t and l_{GR} are the width, thickness and length of graphene, respectively). The advantage of graphene as a reinforcing phase lies in the high specific surface area and high aspect ratio, so ensuring the uniform dispersion of graphene is the key to the effective load transfer mechanism [39].

The existence of a large thermal expansion mismatch between graphene and the matrix causes internal stresses at the interface after sintering, which induces plastic deformation of the matrix, leading to the formation of a high-density dislocation zone near the interface (Fig. 6d). The interaction between dislocations is also an important factor in strength enhancement, and the presence of internal stresses prevents the expansion of cracks perpendicular to them [10]. The increase in yield strength due to thermal expansion mismatch can be expressed as [40]:

$$\Delta\sigma_{CTE} = \alpha G_m b\sqrt{\frac{12\Delta T(C_M - C_{GR})V_{GR}}{bd_{GR}}} \quad (3)$$

where α is a constant(1.25 [40]) and G_m is the shear modulus of the matrix(~ 43 GPa [41]), b is the burger vector of the matrix(~ 0.25 nm [42]), ΔT is the temperature difference, C_M(~ 16×10^{-6} k^{-1} [24]) and C_{GR}(~ 0.9×10^{-6} k^{-1} [24]) are the thermal expansion coefficients of the matrix and graphene, respectively, V_{GR} is the volume fraction of

graphene(0.8%), and d_{GR} is the average graphene size(assumed to be 300 nm as shown in Figure 6). The calculated value of $\Delta\sigma_{CTE}$ is about 55 MPa. Therefore, the more graphene content, the more pronounced the strengthening effect is when graphene is uniformly dispersed and well bonded to the matrix. In addition, graphene will also act as a barrier to dislocation motion and grain boundary migration [43]. Part of graphene will be distributed at grain boundaries (Fig. 6a), hindering the migration of grain boundaries, which can effectively limit the growth of grains during the sintering process. Grain boundaries are a large barrier to dislocation motion (Fig. 6i), and the total grain boundary area of the refined grains increases, which increases the obstruction to dislocation motion and thus achieves the purpose of improving strength.

As shown in Fig. 7c, the strength of the laminated composites containing 0.25 wt.% graphene is greatly improved, while the plasticity is only slightly decreased compared with the alloy. Combined with the results of the previous study [29], the reason why the CuAlMn alloys can maintain good plasticity while improving strength lies in the laminar structure. In the laminar structure, graphene as a "mortar" is uniformly filled in the CuAlMn matrix, on the one hand, it can play the internal toughening mechanism, graphene around the "bricks" can be sliding within a small range when subjected to external forces, resulting in limited inelastic deformation, so as to alleviate the stress concentration, to avoid the emergence of cracks [14]. When cracks exist, graphene exerts an external toughening mechanism by controlling crack extension, as shown in Fig. 8b, crack extension perpendicular to the layer direction is hindered by graphene, and the crack tip bends along the graphene direction, resulting in the extension path changing between perpendicular to the layer and the direction along the layer, which increases the energy required for fracture. At the same time, graphene acts as a bridge to connect the crack surfaces together, hindering crack tensioning. Thus, crack deflection and bridging act as further toughening mechanisms to avoid catastrophic crack extension and allow stable crack growth to improve material toughness [44]. Laminar structures are also helpful in increasing strength, for example, they can improve the interfacial bonding of graphene to the matrix and control the alignment of graphene along the loading direction [45].

4.2. Damping properties enhancement mechanisms

The damping mechanism of CuAlMn alloys includes phase transition damping, interface damping, and dislocation damping, and their damping properties are mainly related to the martensitic structure [46], as can be seen in Fig. 5, there are profuse stacking faults inside the martensite, and the interfaces provided by the stacking faults play an important role in the damping mechanism of the alloys [47]. The addition of graphene has a large effect on interfacial and dislocation damping. Since the damping properties are tested at room temperature, there is no involvement of phase transition damping, and intrinsic damping, dislocation damping, and matrix/graphene interfacial damping play a major role.

The addition of graphene introduces a large number of microscopic defects into the metal matrix, which is an important factor in the enhancement of damping properties [1]. The large thermal expansion coefficient difference between graphene and CuAlMn alloys mentioned above creates a high density of dislocation regions on one side of the matrix (Fig. 6d), and dislocation motion at low amplitudes is the main mode of energy dissipation. Defect regions such as grain boundaries in the matrix can have an effect on the dislocation motion, and the Granato-Lucke (G-L) theory illustrates the mechanism of dislocation-defect interaction [8]. A schematic diagram of the G-L mechanism (Fig. 10b) is made according to Fig. 10a, where the grain boundary acts as a strong pinning point pinned on the dislocation line and acts as an obstacle to dislocation motion. Under external stress, the dislocation line oscillates between pinned points, when the amplitude is small, the dislocations can only oscillate between weakly pinned points such as vacancies and impurities, moving a limited distance and contributing less to damping. As the strain amplitude increases, the dislocations break away from the binding of weak pinning, and greater displacement bending occurs between the strong pinning points, and the dislocations sweep through a larger area so that more energy can be consumed. Thus the damping produced by dislocations is strain amplitude dependent [48].

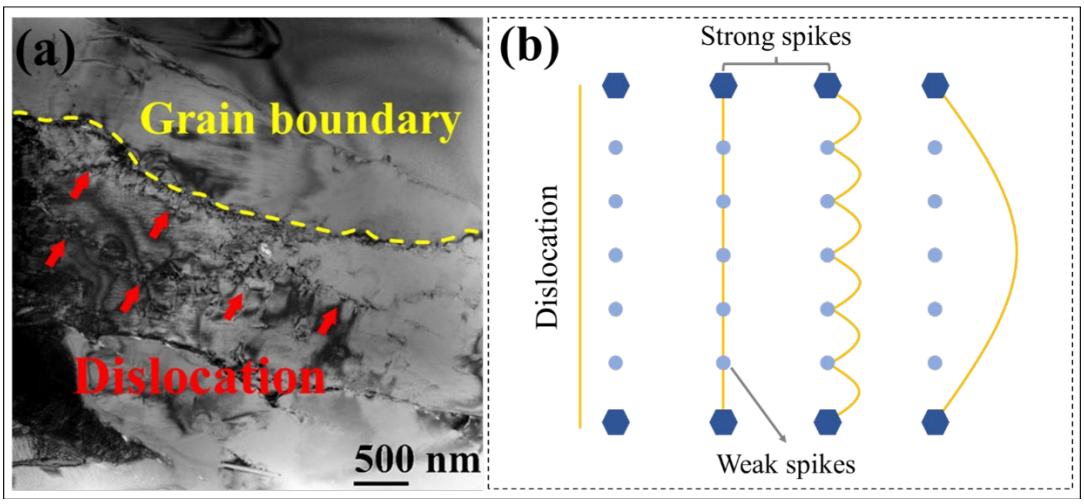

Fig. 10. (a) Dislocation distribution at grain boundaries, (b) Schematic of the G-L mechanism

According to G-L theory, the effect of dislocation motion on damping can be given by the following relation [49]:

$$Q^{-1} = Q_a^{-1} + Q_f^{-1} \tag{4}$$

$$Q_a^{-1} = C_1 \frac{\rho b^2}{\varepsilon_0} \exp\left(-\frac{C_2}{\varepsilon_0}\right) \tag{5}$$

$$Q_f^{-1} = \frac{C_3 \rho f^2}{b^2} \tag{6}$$

$$\ln(Q_a^{-1} \times \varepsilon_0) = \ln(C_1 \rho b^2) - \frac{C_2}{\varepsilon_0} \tag{7}$$

where C_1, C_2 and C_3 are physical constants, ρ is the dislocation density, b is the Burgers vector, ε_0 and f are the vibrational strain amplitude and frequency, respectively. Q_a^{-1} is the amplitude-dependent damping, Q_f^{-1} is the frequency-dependent damping. Q_f^{-1} dominates at low amplitudes, and after the amplitude exceeds the critical value, the damping value mainly originates from Q_a^{-1}. Converting Eq. (5) to Eq. (7) yields a negative correlation between $\ln(Q_a^{-1} \times \varepsilon_0)$ and $1/\varepsilon_0$, and the curves are plotted according to the obtained data (Fig. 11), from which it can be seen that in the low-amplitude region $\ln(Q_a^{-1} \times \varepsilon_0)$ and $1/\varepsilon_0$ have a basically linear correlation, and in the high amplitude region, the effect of interface damping is higher than that of dislocation damping, so the curves no longer have a linear relationship.

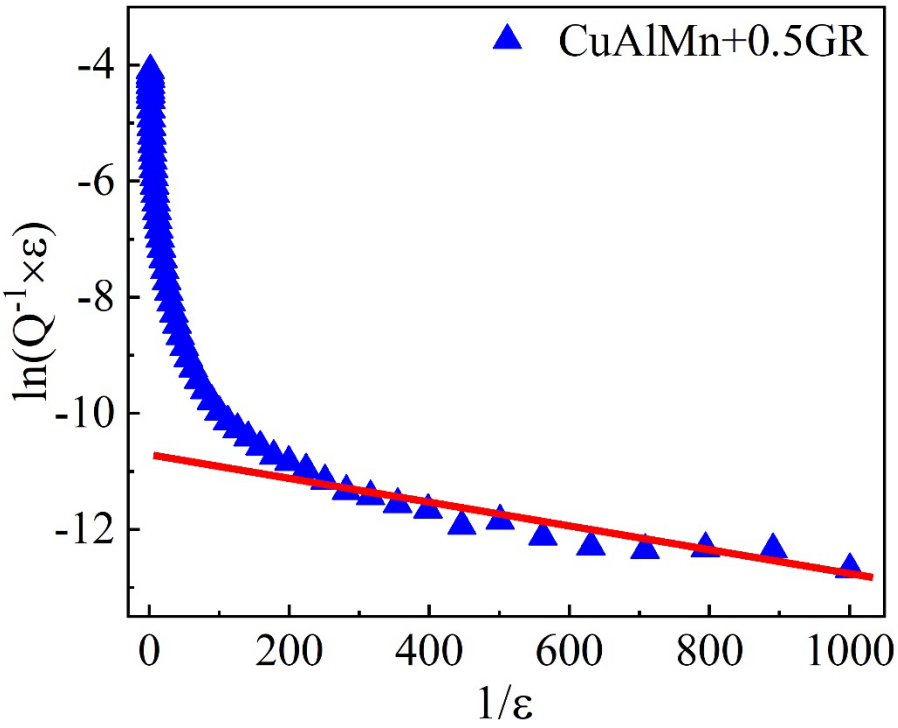

Fig. 11. G-L curves for CuAlMn + 0.5 wt.% GR samples

The presence of graphene forms a large number of microscopic interfaces, and the sliding between the interfaces at high amplitudes is an important way to dissipate energy, which is another factor for the increase of damping [11]. The wettability of graphene and CuAlMn alloys is very poor, and the bonding interface has no product, which relies solely on mechanical interlocking and weak bonding strength [50], so the interface between graphene and matrix is prone to sliding friction when the shear stress at the interface is large. Because graphene has a large specific surface area [51], and the laminar structure allows the graphene to have a larger displacement distance, the sliding friction at the graphene/matrix interface can dissipate a large amount of energy. As the graphene content increases and the graphene is stacked into multilayers of graphene with weak van der Waals forces connecting the layers, which results in sliding not only at the graphene/matrix interface, but also between the graphene layers and thus increases the energy dissipation [50].

5. Conclusion

$(CuAlMn)_{1-x}GR_x$ laminated composites were prepared by sheet powder metallurgy with vacuum hot pressing method, and the effect of graphene content on microstructure, mechanical properties and damping properties of CuAlMn alloys was investigated. The

following conclusions can be drawn:

1. When graphene content was added up to 0.25 wt.%, the tensile strength and microhardness of the composites reached 423 MPa and 269 HV, which were enhanced by about 17% and 27%, respectively, and elongation of about 17% was maintained. The damping properties improved with the increase of graphene content, and the damping value of the 0.25 wt.% graphene sample was about 25% higher compared to the alloy at a frequency of 1 Hz and 600 μm amplitude. The results show that the addition of a small amount of graphene can simultaneously improve the mechanical and damping properties of the material.

2. The composites can maintain good elongation lies in the toughening mechanism of the laminar structure. The mechanism of graphene's enhancement of the strength of the composites is mainly the load transfer, and the high-density dislocation zone caused by the thermal expansion mismatch is also an important reason for the improvement of the strength.

3. Dislocation damping and interface damping are the main damping mechanisms in composites. Dislocations mainly originate from the matrix plastic deformation caused by the thermal expansion mismatch, which is the source of damping at low amplitudes; at high amplitudes, graphene/matrix interface motion becomes the main mode of energy dissipation, acting in conjunction with dislocation damping.

Conflict of interest

The authors declare that they have no conflict of interest.

Acknowledgments

This work was supported by Key Laboratory of Infrared Imaging Materials and Detectors, Shanghai Institute of Technical Physics, Chinese Academy of Sciences (No. IIMDKFJJ-21-10) and China Postdoctoral Science Foundation (No. 2018T110993). We would like to thank Analytical and Testing Center of Southwest Jiaotong University for partial testing.

Data Availability statement

The data used to support the findings of this study are available from the corresponding author upon request.

References

[1] Zhang J, Perez R J, Wong C R, et al. Effects of secondary phases on the damping behaviour of metals, alloys and metal matrix composites[J]. Materials Science and Engineering: R: Reports, 1994, 13(8): 325-389. https://doi.org/10.1016/0927-796x(94)90010-8

[2] Saedi S, Acar E, Raji H, et al. Energy Damping in Shape Memory Alloys: A Review[J]. Journal of Alloys and Compounds, 2023: 170286. https://doi.org/10.1016/j.jallcom.2023.170286

[3] Sun L, Huang W M, Ding Z, et al. Stimulus-responsive shape memory materials: a review[J]. Materials & Design, 2012, 33: 577-640. https://doi.org/10.1016/j.matdes.2011.04.065

[4] Sutou Y, Omori T, Wang J J, et al. Characteristics of Cu–Al–Mn-based shape memory alloys and their applications[J]. Materials Science and Engineering: A, 2004, 378(1-2): 278-282. https://doi.org/10.1016/j.msea.2003.12.048

[5] Gholami-Kermanshahi M, Wu Y Y, Lange G, et al. Effect of alloying elements (Nb, Ag) on the damping performance of Cu–Al–Mn shape memory alloys[J]. Journal of Alloys and Compounds, 2023, 930: 167438. https://doi.org/10.1016/j.jallcom.2022.167438

[6] Chang S H. Influence of chemical composition on the damping characteristics of Cu–Al–Ni shape memory alloys[J]. Materials Chemistry and Physics, 2011, 125(3): 358-363. https://doi.org/10.1016/j.matchemphys.2010.09.077

[7] Yang L, Jiang X, Sun H, et al. Effects of alloying, heat treatment and nanoreinforcement on mechanical properties and damping performances of Cu–Al-based alloys: A review[J]. Nanotechnology Reviews, 2021, 10(1): 1560-1591. https://doi.org/10.1515/ntrev-2021-0101

[8] Yang G, Han Y, Lu A, et al. Enhanced damping capacity of nanolaminated graphene (reduced graphene oxide)/Al-Mg-Si composite[J]. Composites Part A: Applied Science and Manufacturing, 2022, 156: 106887. https://doi.org/10.1016/j.compositesa.2022.106887

[9] Katsiropoulos C V, Pappas P, Koutroumanis N, et al. Enhancement of damping

response in polymers and composites by the addition of graphene nanoplatelets[J]. Composites Science and Technology, 2022, 227: 109562. https://doi.org/10.1016/j.compscitech.2022.109562

[10] Chen F, Ying J, Wang Y, et al. Effects of graphene content on the microstructure and properties of copper matrix composites[J]. Carbon, 2016, 96: 836-842. https://doi.org/10.1016/j.carbon.2015.10.023

[11] Jiao Z, Wang Q, Yin F, et al. Novel laminated multi-layer graphene/Cu–Al–Mn composites with ultrahigh damping capacity and superior tensile mechanical properties[J]. Carbon, 2022, 188: 45-58. https://doi.org/10.1016/j.carbon.2021.11.055

[12] Li Z, Guo Q, Li Z, et al. Enhanced mechanical properties of graphene (reduced graphene oxide)/aluminum composites with a bioinspired nanolaminated structure[J]. Nano Letters, 2015, 15(12): 8077-8083. https://doi.org/10.1021/acs.nanolett.5b03492

[13] Walther A, Bjurhager I, Malho J M, et al. Large-area, lightweight and thick biomimetic composites with superior material properties via fast, economic, and green pathways[J]. Nano Letters, 2010, 10(8): 2742-2748. https://doi.org/10.1021/nl1003224

[14] Ritchie R O. The conflicts between strength and toughness[J]. Nature Materials, 2011, 10(11): 817-822. https://doi.org/10.1038/nmat3115

[15] Jiang L, Li Z, Fan G, et al. A flake powder metallurgy approach to Al_2O_3/Al biomimetic nanolaminated composites with enhanced ductility[J]. Scripta Materialia, 2011, 65(5): 412-415. https://doi.org/10.1016/j.scriptamat.2011.05.022

[16] Jiang L, Fan G, Li Z, et al. An approach to the uniform dispersion of a high volume fraction of carbon nanotubes in aluminum powder[J]. Carbon, 2011, 49(6): 1965-1971. https://doi.org/10.1016/j.carbon.2011.01.021

[17] Wang H, Zhang H M, Cheng X W, et al. Effect of ball milling time on microstructure and mechanical properties of graphene nanoplates and TiBw reinforced Ti–6Al–4V alloy composites[J]. Materials Science and Engineering: A, 2022, 861: 144240. https://doi.org/10.1016/j.msea.2022.144240

[18] Dixit M, Srivastava R. The effect of copper granules on interfacial bonding and properties of the copper-graphite composite prepared by flake powder metallurgy[J]. Advanced Powder Technology, 2019, 30(12): 3067-3078.

https://doi.org/10.1016/j.apt.2019.09.013

[19] Varol T, Canakci A. The effect of type and ratio of reinforcement on the synthesis and characterization Cu-based nanocomposites by flake powder metallurgy[J]. Journal of Alloys and Compounds, 2015, 649: 1066-1074. https://doi.org/10.1016/j.jallcom.2015.07.008

[20] Li Y W, Xiao L R, Zhang W, et al. Microstructure and mechanical properties of aluminum bronze with different Mn contents[J]. Chinese Journal of Rare Metals, 2017, 41: 985-991. https://doi.org/10.13373/j.cnki.cjrm.XY16032902

[21] Zhang G, Yin H, Zhang C, et al. Effect of Mn on microstructure and properties of Cu-12Al powder metallurgy alloy[J]. Materials Research Express, 2020, 7(1): 016546. https://doi.org/10.1088/2053-1591/ab63f8

[22] Salvo C, Mangalaraja R V, Udayabashkar R, et al. Enhanced mechanical and electrical properties of novel graphene reinforced copper matrix composites[J]. Journal of Alloys and Compounds, 2019, 777: 309-316. https://doi.org/10.1016/j.jallcom.2018.10.357

[23] Gao X, Yue H, Guo E, et al. Mechanical properties and thermal conductivity of graphene reinforced copper matrix composites[J]. Powder Technology, 2016, 301: 601-607. https://doi.org/10.1016/j.powtec.2016.06.045

[24] Wang Q Z, Han F S, Wu J, et al. Thermal stresses in a macroscopic graphite particulates reinforced CuAlMn shape memory alloy studied by internal friction[J]. Materials Science and Engineering: A, 2005, 408(1-2): 247-254. https://doi.org/10.1016/j.msea.2005.08.010

[25] Pandey A, Hussain S, Nair P, et al. Influence of niobium and silver on mechanical properties and shape memory behavior of Cu-12Al-4Mn alloys[J]. Journal of Alloys and Compounds, 2020, 836: 155266. https://doi.org/10.1016/j.jallcom.2020.155266

[26] Adorno A T, Silva R A G. Ageing behavior in the Cu–10 wt.% Al and Cu–10 wt.% Al–4 wt.% Ag alloys[J]. Journal of Alloys and Compounds, 2009, 473(1-2): 139-144. https://doi.org/10.1016/j.jallcom.2008.05.072

[27] Zhang Y, Xu L, Zhao L, et al. Process-microstructure-properties of CuAlNi shape memory alloys fabricated by laser powder bed fusion[J]. Journal of Materials Science

& Technology, 2023, 152: 1-15. https://doi.org/10.1016/j.jmst.2022.12.037

[28] Kim T H, Ouyang G, Poplawsky J D, et al. In-situ TEM analysis of the phase transformation mechanism of a Cu–Al–Ni shape memory alloy[J]. Journal of Alloys and Compounds, 2019, 808: 151743. https://doi.org/10.1016/j.jallcom.2019.151743

[29] Yang L, Jiang X, Sun H, et al. Effect of Ta addition on microstructures, mechanical and damping properties of Cu–Al–Mn–Ti alloy[J]. Journal of Materials Research and Technology, 2021, 15: 3825-3835. https://doi.org/10.1016/j.jmrt.2021.10.031

[30] Zheng Z, Yang X, Li J, et al. Preparation and properties of graphene nanoplatelets reinforced aluminum composites[J]. Transactions of Nonferrous Metals Society of China, 2021, 31(4): 878-886. https://doi.org/10.1016/s1003-6326(21)65546-2

[31] Chen Y, Zhang X, Liu E, et al. Fabrication of in-situ grown graphene reinforced Cu matrix composites[J]. Scientific Reports, 2016, 6(1): 19363. https://doi.org/10.1038/srep19363

[32] Zhao Z, Bai P, Du W, et al. An overview of graphene and its derivatives reinforced metal matrix composites: Preparation, properties and applications[J]. Carbon, 2020, 170: 302-326. https://doi.org/10.1016/j.carbon.2020.08.040

[33] Yue H, Yao L, Gao X, et al. Effect of ball-milling and graphene contents on the mechanical properties and fracture mechanisms of graphene nanosheets reinforced copper matrix composites[J]. Journal of Alloys and Compounds, 2017, 691: 755-762. https://doi.org/10.1016/j.jallcom.2016.08.303

[34] Tang Z, Li G, Lu S, et al. Enhance mechanical damping behavior of RHA-cement mortar with bionic inorganic-organic laminated structures[J]. Construction and Building Materials, 2022, 323: 126521. https://doi.org/10.1016/j.conbuildmat.2022.126521

[35] Dang C, Wang J, Wang J, et al. An ultrahigh strain-independent damping capacity in Mg–1Mn alloy by cold rolling process[J]. Journal of Materials Research and Technology, 2023, 25: 4330-4341. https://doi.org/10.1016/j.jmrt.2023.06.086

[36] Ma Y, Liu C, Jiang S, et al. Tailoring good combinations among strength, ductility and damping capacity in a novel Mg-1.5Gd–1Zn damping alloy via hot extrusion[J]. Materials Science and Engineering: A, 2023, 871: 144827.

https://doi.org/10.1016/j.msea.2023.144827

[37] Shin S E, Choi H J, Shin J H, et al. Strengthening behavior of few-layered graphene/aluminum composites[J]. Carbon, 2015, 82: 143-151. https://doi.org/10.1016/j.carbon.2014.10.044

[38] Guo S, Zhang X, Shi C, et al. Simultaneously enhanced mechanical properties and electrical property of Cu-2 wt% Ag alloy matrix composites with analogy-bicontinuous structures constructed via in-situ synthesized graphene nanoplatelets[J]. Carbon, 2022, 198: 207-218. https://doi.org/10.1016/j.carbon.2022.07.025

[39] Chen Z H, Hui H Y, Li C L, et al. GNPs/Al nanocomposites with high strength and ductility and electrical conductivity fabricated by accumulative roll-compositing[J]. Rare Metals, 2021, 40: 2593-2601. https://doi.org/10.1007/s12598-020-01695-9

[40] Chen H, Mi G, Li P, et al. Excellent high-temperature strength and ductility of graphene oxide reinforced high-temperature titanium alloy matrix composite fabricated by hot isostatic pressing and heat treatment[J]. Composites Communications, 2022, 30: 101077. https://doi.org/10.1016/j.coco.2022.101077

[41] Yang J, Ouyang P, Liu T, et al. First-principles study of the effect of aluminum content on the elastic properties of Cu-Al alloys[J]. Materials Today Communications, 2022, 31: 103399. https://doi.org/10.1016/j.mtcomm.2022.103399

[42] Wang J J, Tao N R, Lu K. Revealing the deformation mechanisms of nanograins in gradient nanostructured Cu and CuAl alloys under tension[J]. Acta Materialia, 2019, 180: 231-242. https://doi.org/10.1016/j.actamat.2019.09.021

[43] Nieto A, Bisht A, Lahiri D, et al. Graphene reinforced metal and ceramic matrix composites: a review[J]. International Materials Reviews, 2017, 62(5): 241-302. https://doi.org/10.1080/09506608.2016.1219481

[44] Hassan H A, Lewandowski J J. Laminated nanostructure composites with improved bend ductility and toughness[J]. Scripta Materialia, 2009, 61(11): 1072-1074. https://doi.org/10.1016/j.scriptamat.2009.08.034

[45] Cao M, Xiong D B, Tan Z, et al. Aligning graphene in bulk copper: Nacre-inspired nanolaminated architecture coupled with in-situ processing for enhanced mechanical properties and high electrical conductivity[J]. Carbon, 2017, 117: 65-74.

https://doi.org/10.1016/j.carbon.2017.02.089

[46] Gholami-Kermanshahi M, Wu Y Y, Lange G, et al. Effect of alloying elements (Nb, Ag) on the damping performance of Cu–Al–Mn shape memory alloys[J]. Journal of Alloys and Compounds, 2023, 930: 167438. https://doi.org/10.1016/j.jallcom.2022.167438

[47] Xu C, Zhang J, Liu S, et al. Microstructure, mechanical and damping properties of Mg–Er–Gd–Zn alloy reinforced with stacking faults[J]. Materials & Design, 2015, 79: 53-59. https://doi.org/10.1016/j.matdes.2015.04.037

[48] Wang Q Z, Han F S, Wu J, et al. Effects of macroscopic defects on the damping behavior of CuAlMn shape memory alloy[J]. Journal of Alloys and Compounds, 2006, 425(1-2): 200-205. https://doi.org/10.1016/j.jallcom.2006.01.062

[49] Gu J, Zhang X, Gu M, et al. Internal friction peak and damping mechanism in high damping 6061Al/SiCp/Gr hybrid metal matrix composite[J]. Journal of Alloys and Compounds, 2004, 372(1-2): 304-308. https://doi.org/10.1016/j.jallcom.2003.10.021

[50] Lin G, Peng Y, Li Y, et al. Remarkable anisotropic wear resistance with 100-fold discrepancy in a copper matrix laminated composite with only 0.2 vol% graphene[J]. Acta Materialia, 2021, 215: 117092. https://doi.org/10.1016/j.actamat.2021.117092

[51] Güler Ö, Bağcı N. A short review on mechanical properties of graphene reinforced metal matrix composites[J]. Journal of Materials Research and Technology, 2020, 9(3): 6808-6833. https://doi.org/10.1016/j.jmrt.2020.01.077